Superconductivity in monolayer FeSe enhanced by quantum geometry

Taisei Kitamura ⬤,[1,*] Tatsuya Yamashita,[1] Jun Ishizuka ⬤,[2] Akito Daido ⬤,[1] and Youichi Yanase[1,3]

[1]*Department of Physics, Graduate School of Science, Kyoto University, Kyoto 606-8502, Japan*
[2]*Institute for Theoretical Physics, ETH Zurich, 8093 Zurich, Switzerland*
[3]*Institute for Molecular Science, Okazaki 444-8585, Japan*

We formulate the superfluid weight in unconventional superconductors with $\boldsymbol{k}$-dependent Cooper pair potentials based on the geometric properties of Bloch electrons. We apply the formula to a model of monolayer FeSe obtained by first-principles calculation. Our numerical calculations point to a significant enhancement of the Berezinskii-Kosterlitz-Thouless transition temperature due to the geometric contribution to the superfluid weight, which is not included in the Fermi liquid theory. The $\boldsymbol{k}$ dependence of the gap function also stabilizes the superconducting state. Our results reveal that the geometric properties of Bloch electrons play an essential role in superconducting materials and pave the way for clarifying hidden aspects of superconductivity from the viewpoint of quantum geometry.

I. INTRODUCTION

Monolayer FeSe grown on $SrTiO_3$ has been reported to experience a superconducting transition at the transition temperature T_c higher than 65 K [1–3] in stark contrast to $T_c \sim 8$ K of the bulk FeSe [4]. Such a significant enhancement of transition temperature has attracted much attention, and it is pointed out that the film thickness [5] and the effect of the substrate [6–9] are essential in the enhancement of the superconducting mean-field transition temperature. However, this high-temperature superconductivity in monolayer FeSe remains to be an unclarified issue as follows.

In two-dimensional superconductors, the resistive transition is determined by the Berezinskii-Kosterlitz-Thouless (BKT) transition [10,11], where the BKT transition temperature T_{BKT} is given by the superfluid weight $D^{\mathrm{s}}(T)$ according to the formula $D^{\mathrm{s}}(T_{\mathrm{BKT}}) = 8T_{\mathrm{BKT}}/\pi$ [12–14]. Considering that superconductivity emerges with the BKT transition, the study of the BKT transition and the superfluid weight is another key issue, different from studies of the mean-field transition temperature, to understanding the high-temperature superconductivity in monolayer FeSe. It should also be noted that the superfluid weight is essential for the Meissner effect and is related to the magnetic penetration depth by $\lambda(T) = 1/\sqrt{4\pi D^{\mathrm{s}}(T)}$. Considering the temperature dependence of $D^{\mathrm{s}}(T)$ and $\lambda(T)$ is closely related to the gap structure , the superfluid weight is a useful probe of the pairing symmetry [15–19]. Thus, the evaluation of the superfluid weight is essential to explore the nature of high-temperature superconductivity in monolayer FeSe.

In the Fermi-liquid theory, the superfluid weight has been believed to be determined by the density of electrons n^* and the effective mass m^*, i.e., n^*/m^* [20–22]. However, recent studies have revealed that the geometric properties of Bloch electrons can contribute to the superfluid weight in multiband superconductors [23,24]. When the bands are sufficiently apart from each other, this contribution reduces to the quantum metric of the Bloch wave function [24].

The quantum metric is closely related to the Berry curvature through the quantum geometric tensor [25,26]. The imaginary part of the quantum geometric tensor is widely known as the Berry curvature [27], which appears in various Hall responses [28–30]. The real part is the quantum metric, which also appears in physical properties of solids [31–37]. The quantum metric can be divided into the contribution from each band, which is specially called the band-resolved quantum metric. The band-resolved quantum metric has been revealed to be an essential ingredient of nonlinear optical responses [38,39]. The quantum geometry is a purely interband effect of Bloch electrons, which comes from mixing degrees of freedom, such as the orbitals.

The importance of the geometric contribution to the superfluid weight was discussed for the first time in the Lieb optical lattice of cold atoms [40,41], where the flat band has been realized [42,43]. In the flat-band limit, the conventional contribution disappears because $m^* \to \infty$ leads to $n^*/m^* \to 0$; this implies the dominant geometric contribution. Furthermore, in superconducting twisted bilayer graphene [44], in which the moiré flat-band appears [45,46], the geometric contribution is shown to be dominant [47–50]. Thus, an essential role of the geometric properties of Bloch electrons has been recognized for the superconductivity in artificial quantum systems.

In this paper, we show that the monolayer FeSe on $SrTiO_3$ with high transition temperature manifests the geometric contribution to the superfluid weight without artificial electronic structure. Because FeSe is a multiband superconductor

*kitamura.taisei.67m@st.kyoto-u.ac.jp

and the mother compound of a topological superconductor candidate FeSe$_{1-x}$Te$_x$ [51–55], the geometric properties of Bloch electrons should be nontrivial and may cause intriguing phenomena. Furthermore, FeSe has a small carrier density n^*, and thus in the Bardeen-Cooper-Schrieffer to Bose-Einstein-Condensation (BCS-BEC) crossover regime [56–60]. Therefore, the geometric contribution to the superfluid weight is naturally expected to have a significant effect on the superconducting FeSe. Thus, FeSe may offer a promising platform to study the geometric effects in nonartificial superconductors.

II. FORMULATION OF SUPERFLUID WEIGHT

In the previous study based on the BCS theory [24], the superfluid weight with the $\boldsymbol{k}$-independent pairing is divided into two terms: One is the conventional term while the other is the geometric term. We extend the formulation to describe unconventional superconductivity. The superfluid weight will be divided into four terms as will be shown later in Eqs. (4)–(8).

We start from the Bogoliubov–de Gennes (BdG) Hamiltonian, $\hat{H}_{\mathrm{BdG}} = \sum_{\boldsymbol{k}} \hat{\psi}_{\boldsymbol{k}}^{\dagger} H_{\mathrm{BdG}\boldsymbol{k}} \hat{\psi}_{\boldsymbol{k}}$, with

$$H_{\mathrm{BdG}\boldsymbol{k}} = \begin{pmatrix} H_{0\boldsymbol{k}} & \boldsymbol{\Delta}_{\boldsymbol{k}} \\ \boldsymbol{\Delta}_{\boldsymbol{k}}^{\dagger} & -H_{0-\boldsymbol{k}}^{T} \end{pmatrix}, \tag{1}$$

where $\boldsymbol{k}$ is the wave vector and $\hat{\psi}_{\boldsymbol{k}}$ is the Nambu spinor written by $\hat{\psi}_{\boldsymbol{k}} = (\hat{c}_{1\uparrow\boldsymbol{k}}, \cdots, \hat{c}_{f\uparrow\boldsymbol{k}}, \hat{c}_{1\downarrow-\boldsymbol{k}}^{\dagger}, \cdots, \hat{c}_{f\downarrow-\boldsymbol{k}}^{\dagger})^{T}$. Here, $\hat{c}_{i\sigma\boldsymbol{k}}^{\dagger}$ ($\hat{c}_{i\sigma\boldsymbol{k}}$) is the creation (annihilation) operator, $i = 1, 2, \cdots f$ shows the orbital and sublattice indices, and $\sigma = \uparrow, \downarrow$ represents the spin. We ignore the spin-orbit coupling and assume spin-singlet superconductivity with iron-based superconductors in mind. $H_{0\boldsymbol{k}}$ and $\boldsymbol{\Delta}_{\boldsymbol{k}}$ are the matrix representation of the Fourier transform of hopping integrals and the gap function, respectively.

The current response of superconductors to the vector potential $A_{\mu}(\boldsymbol{q}, \omega)$ is described by the Meissner kernel $K_{\mu\nu}(\boldsymbol{q}, \omega)$, as $j_{\mu}(\boldsymbol{q}, \omega) = -K_{\mu\nu}(\boldsymbol{q}, \omega)A_{\nu}(\boldsymbol{q}, \omega)$. The superfluid weight $D_{\mu\nu}^{\mathrm{s}}$ is defined by its q limit, $D_{\mu\nu}^{\mathrm{s}} = \lim_{\boldsymbol{q}\to 0} K_{\mu\nu}(\boldsymbol{q}, 0)$. According to the Kubo formula, the superfluid weight is obtained as

$$\begin{aligned} D_{\mu\nu}^{\mathrm{s}} = \sum_{\boldsymbol{k}\alpha\beta} &\frac{f(E_{\alpha\boldsymbol{k}}) - f(E_{\beta\boldsymbol{k}})}{E_{\alpha\boldsymbol{k}} - E_{\beta\boldsymbol{k}}} \\ &\times (\langle \psi_{\alpha\boldsymbol{k}} | \partial_{\mu} H_{p\boldsymbol{k}} | \psi_{\beta\boldsymbol{k}} \rangle \langle \psi_{\beta\boldsymbol{k}} | \partial_{\nu} H_{p\boldsymbol{k}} | \psi_{\alpha\boldsymbol{k}} \rangle \\ &- \langle \psi_{\alpha\boldsymbol{k}} | \partial_{\mu} H_{\mathrm{BdG}\boldsymbol{k}} | \psi_{\beta\boldsymbol{k}} \rangle \langle \psi_{\beta\boldsymbol{k}} | \partial_{\nu} H_{m\boldsymbol{k}} | \psi_{\alpha\boldsymbol{k}} \rangle), \end{aligned} \tag{2}$$

where we introduced block-diagonal matrices:

$$H_{p(m)\boldsymbol{k}} = \begin{pmatrix} H_{0\boldsymbol{k}} & 0 \\ 0 & (-)H_{0-\boldsymbol{k}}^{T} \end{pmatrix}. \tag{3}$$

The wave function and the energy eigenvalue of the BdG Hamiltonian are denoted by $H_{\mathrm{BdG}\boldsymbol{k}} | \psi_{\alpha\boldsymbol{k}} \rangle = E_{\alpha\boldsymbol{k}} | \psi_{\alpha\boldsymbol{k}} \rangle$.

To classify the superfluid weight by the geometric properties of the normal state, we introduce the energy and the Bloch wave function, i.e., $H_{0\boldsymbol{k}} | u_{n\boldsymbol{k}} \rangle = \epsilon_{n\boldsymbol{k}} | u_{n\boldsymbol{k}} \rangle$, following Ref. [24]. For simplicity, we assume the time-reversal symmetry, under which $H_{0\boldsymbol{k}} = H_{0-\boldsymbol{k}}^{T}$ is satisfied. Using the matrix elements $\phi_{n\boldsymbol{k}}^{i\uparrow(\downarrow)}$ of the unitary matrix which diagonalizes the BdG

Hamiltonian, the wave function of the BdG Hamiltonian is expanded by the normal state Bloch wave function as $|\psi_{\alpha\boldsymbol{k}}\rangle = (\sum_n \phi_{n\boldsymbol{k}}^{\alpha\uparrow} | u_{n\boldsymbol{k}} \rangle \quad \sum_n \phi_{n\boldsymbol{k}}^{\alpha\downarrow} | u_{n\boldsymbol{k}} \rangle)^{T}$. By using this relationship, the superfluid weight for unconventional superconductors is divided into four parts as follows:

$$D_{\mu\nu}^{\mathrm{s}} = D_{\mu\nu}^{\mathrm{conv}} + D_{\mu\nu}^{\mathrm{geom}} + D_{\mu\nu}^{\mathrm{multi}} + D_{\mu\nu}^{\mathrm{gap}}, \tag{4}$$

$$D_{\mu\nu}^{\mathrm{conv}} = 2 \sum_{nm\boldsymbol{k}} C_{nnmm\boldsymbol{k}}^{\uparrow\uparrow\downarrow\downarrow} (J_{nn\boldsymbol{k}}^{\mu} J_{mm\boldsymbol{k}}^{\nu} + J_{nn\boldsymbol{k}}^{\nu} J_{mm\boldsymbol{k}}^{\mu}), \tag{5}$$

$$D_{\mu\nu}^{\mathrm{geom}} = 2 \sum_{n\neq m, l\neq s\boldsymbol{k}} C_{nml s\boldsymbol{k}}^{\uparrow\uparrow\downarrow\downarrow} (J_{nm\boldsymbol{k}}^{\mu} J_{ls\boldsymbol{k}}^{\nu} + J_{nm\boldsymbol{k}}^{\nu} J_{ls\boldsymbol{k}}^{\mu}), \tag{6}$$

$$\begin{aligned} D_{\mu\nu}^{\mathrm{multi}} = 2 \sum_{nl\neq s\boldsymbol{k}} \big(&C_{nnl s\boldsymbol{k}}^{\uparrow\uparrow\downarrow\downarrow} (J_{nn\boldsymbol{k}}^{\mu} J_{ls\boldsymbol{k}}^{\nu} + J_{nn\boldsymbol{k}}^{\nu} J_{ls\boldsymbol{k}}^{\mu}) \\ &+ C_{lsnn\boldsymbol{k}}^{\uparrow\uparrow\downarrow\downarrow} (J_{ls\boldsymbol{k}}^{\mu} J_{nn\boldsymbol{k}}^{\nu} + J_{ls\boldsymbol{k}}^{\nu} J_{nn\boldsymbol{k}}^{\mu}) \big), \end{aligned} \tag{7}$$

$$D_{\mu\nu}^{\mathrm{gap}} = \sum_{nml s\sigma\boldsymbol{k}} S \big(C_{nml s\boldsymbol{k}}^{\uparrow\downarrow\sigma\sigma} \delta\Delta_{nm\boldsymbol{k}}^{\mu} + C_{nml s\boldsymbol{k}}^{\downarrow\uparrow\sigma\sigma} \delta\Delta_{nm\boldsymbol{k}}^{\dagger\mu} \big) J_{ls\boldsymbol{k}}^{\nu}, \tag{8}$$

where S takes $-(+)$ when $\sigma = \uparrow(\downarrow)$. Here, $J_{nm\boldsymbol{k}}^{\mu} = \langle u_{n\boldsymbol{k}} | \partial_{\mu} H_{0\boldsymbol{k}} | u_{m\boldsymbol{k}} \rangle$, $\delta\Delta_{nm\boldsymbol{k}}^{(\dagger)}\mu = \langle u_{n\boldsymbol{k}} | \partial_{\mu} \boldsymbol{\Delta}_{\boldsymbol{k}}^{(\dagger)} | u_{m\boldsymbol{k}} \rangle$ and

$$C_{nml s\boldsymbol{k}}^{\sigma_1\sigma_2\sigma_3\sigma_4} = \sum_{\alpha\beta} \frac{f(E_{\alpha\boldsymbol{k}}) - f(E_{\beta\boldsymbol{k}})}{E_{\alpha\boldsymbol{k}} - E_{\beta\boldsymbol{k}}} \phi_{n\boldsymbol{k}}^{\alpha\sigma_1 *} \phi_{m\boldsymbol{k}}^{\beta\sigma_2} \phi_{l\boldsymbol{k}}^{\beta\sigma_3 *} \phi_{s\boldsymbol{k}}^{\alpha\sigma_4}. \tag{9}$$

The details of the derivation are shown in Appendix A.

The conventional term $D_{\mu\nu}^{\mathrm{conv}}$ is found in the first term of Eq. (4). Since $J_{nn\boldsymbol{k}}^{\mu} = \partial_{\mu}\epsilon_{n\boldsymbol{k}}$, this term is essentially determined by the energy dispersion. Only this term is studied in the Fermi-liquid theory. The second term $D_{\mu\nu}^{\mathrm{geom}}$ of Eq. (4) is the interband effect. This term is called the geometric term, as the interband velocity operator appears in Eq. (6), $J_{nm\boldsymbol{k}}^{\mu} = (\epsilon_m - \epsilon_n) \langle u_{n\boldsymbol{k}} | \partial_{\mu} u_{m\boldsymbol{k}} \rangle$, which represents the geometric properties of the Bloch wave function. In the absence of the interband pairing, the terms with $n \neq l, m \neq s$ vanish, and Eq. (6) is represented by the band-resolved quantum metric (see Appendix A). The third term $D_{\mu\nu}^{\mathrm{multi}}$, called the multigap term, vanishes in the case of band-independent pairing. We show that this term is negligible in monolayer FeSe later.

The fourth term $D_{\mu\nu}^{\mathrm{gap}}$ of Eq. (4) comes from the $\boldsymbol{k}$ dependence of the gap function and directly reflects the pairing symmetry. We call this term the gap term. This term has been neglected in previous studies [48]. However, various pairing states, such as an extended s-wave [61–72] or nodeless d-wave state [73–75], have been suggested for monolayer FeSe [5,76], where $\boldsymbol{k}$-dependent gap functions are assumed. Furthermore, this term is required to reproduce the conventional formula, $D \propto n^*/m^*$ (see Appendix A).

III. TEN-ORBITAL MODEL

To calculate the superfluid weight of monolayer FeSe, we construct a realistic ten-orbital tight-binding model for Fe $3d$ orbitals. The first-principles electronic structure calculation is performed using the WIEN2k code [77], and the tight-binding models based on the maximally localized Wannier functions [31,78] are constructed by the WANNIER90 code [79]. The presence of two iron atoms in the unit cell doubles the number of orbitals as $2 \times 5 = 10$.
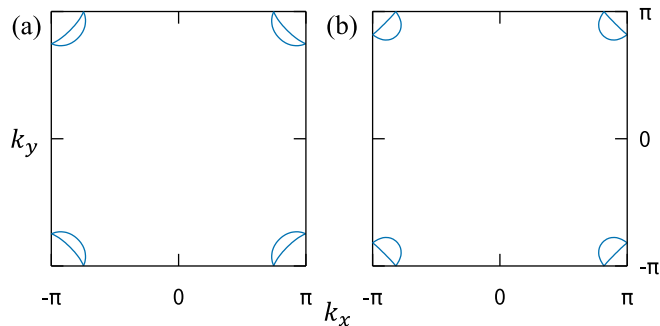
FIG. 1. Fermi surfaces of the model for monolayer FeSe. (a) $n = 6.1$ and (b) 6.06. The holelike Fermi surfaces disappear in all cases.

FIG. 2. Superfluid weight for $\boldsymbol{k}$-independent gap functions. The blue, green, and red lines show the conventional term (D^{conv}), conventional + geometric term ($D^{\text{conv}} + D^{\text{geom}}$), and the total superfluid weight (D^{s}), respectively. The red and green lines almost coincide because D^{multi} is negligible. The purple straight line shows $8T/\pi$ and the intersection with the red line determines the BKT transition temperature. The orange dashed line in panel (a) shows the universal jump of the superfluid weight at $T = T_{\text{BKT}}$. We adopt the renormalization factor $z = 1/5$ in (a) $n = 6.1$, (b) $n = 6.08$, and (c) $n = 6.06$, while $z = 1/8$ and $n = 6.06$ in (d).

We first construct a model of the bulk FeSe. The results of angle-resolved photoemission spectroscopy are known to be slightly different from first-principles calculations [80,81]. To reproduce the experimentally observed Fermi surfaces, we take into account an additional hopping parameter (see Appendix B).

In monolayer FeSe grown on SrTiO$_3$, the holelike Fermi surfaces at Γ point disappear owing to the excess electron doping [82], which can be reproduced by shifting the chemical potential. In this paper, we consider three values for the particle number, $n = 6.1$, 6.08, and 6.06, corresponding to the excess electron doping $n - 6$. The electron doping can also be caused by the K doping [82] and the gate voltage [83,84]. In addition, taking into account the mass enhancement by the electron correlation [80,85,86], we renormalize the normal-state Hamiltonian as $z\hat{H}_0$ instead of the bare one $\hat{H}_0$, with choosing $z = 1/5$ or $1/8$. It is known that the conventional term of the superfluid weight is renormalized by z while the geometric terms are hardly affected. Therefore, the renormalization effect may be essential for the origin of the superfluid weight. The Fermi surfaces of the models are shown in Fig. 1.

IV. SUPERFLUID WEIGHT IN MONOLAYER FESE

In the ten-orbital tight-binding model, the gap functions may be orbital and $\boldsymbol{k}$ dependent, making the multigap and gap terms finite. To determine the gap function and the mean-field transition temperature T_c, we solve the gap equation $\Delta_{ijk} = \sum_{k'} V_{ijkk'} \langle \hat{c}_{j\downarrow-k'} \hat{c}_{i\uparrow k'} \rangle$ self-consistently, with $V_{ijkk'}$ the pairing interaction. We examine some candidates of the pairing state, namely, the s_{++}-wave [61,67,71,72] and incipient $s_{\pm}$-wave [62,68–70] states [63–66]. Qualitatively, the same results are obtained for the d-wave state [73–75] as shown in Appendix C. Furthermore, we study the $\boldsymbol{k}$-independent gap function as well for comparison. For all the cases, we determine the attractive interaction $V_{ijkk'}$ so as to reproduce the mean-field transition temperature $T_c \approx 83$ K because it is considered to be among 65 K to 83 K in monolayer FeSe on SrTiO$_3$ [1–3]. Thus, strong coupling effects, such as an increased electron-phonon coupling by substrates, are phenomenologically included in the high mean-field transition temperature. Similar results are obtained for $T_c = 65$ K as shown in Appendix D.
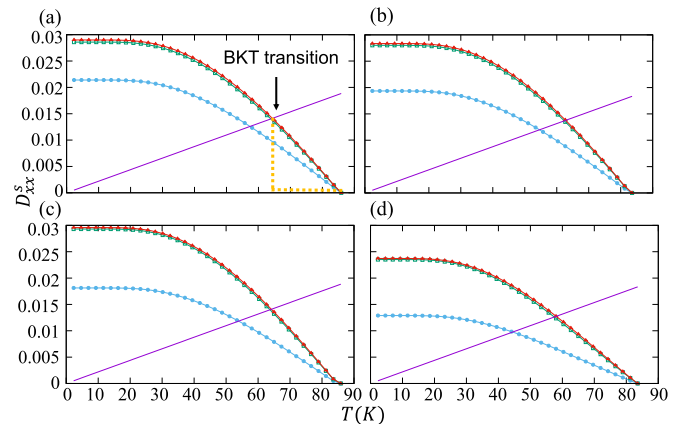
First, we show the results for the $\boldsymbol{k}$-independent gap function, corresponding to the isotropic s-wave superconductivity. We consider an orbital-independent on-site pairing interaction, $V_{ijkk'} = V_0\delta_{ij}$. The gap term $D^{\text{gap}}_{\mu\nu}$ disappears in this case. The temperature dependence of the superfluid weight is shown in Fig. 2. Owing to the fourfold-rotational and mirror symmetries of the system, $D^{\text{s}}_{xx} = D^{\text{s}}_{yy}$ and $D^{\text{s}}_{xy} = 0$ are satisfied. Thus, the BKT transition temperature T_{BKT} is given by the relation $D^{\text{s}}_{xx}(T_{\text{BKT}}) = 8T_{\text{BKT}}/\pi$, and the intersection between the purple straight line and the red solid line indicates the BKT transition temperature. This is also valid for the $\boldsymbol{k}$-dependent gap functions discussed below.

For all parameter sets in Fig. 2, we see a significant geometric contribution to the superfluid weight, whereas the multigap term is negligible in all the results of this paper. While the conventional term is suppressed as expected, the geometric term is enhanced by decreasing the electron number. This contrasting behavior leads to a particularly sizable contribution from the geometric term to the superfluid weight in the low electron-doping region. Accordingly, the geometric term enhances the BKT transition temperature by approximately 24% for the case of $n = 6.06$ and $z = 1/8$, as shown in Fig. 2(d). The geometric term is furthermore significant at low temperatures because the geometric term is higher order in terms of Δ/E_{F}, where Δ is the magnitude of superconducting gap and E_{F} is the Fermi energy. We see that the geometric term determines nearly 45% of the superfluid weight at $T = 0$ in Fig. 2(d). In this parameter set, the superconducting gap on the Fermi surface is approximately 10 meV, consistent with angle-resolved photoemission spectroscopy (ARPES) studies reporting the gap from 8 meV to 20 meV [1–3,82]. These results reveal that the superfluid weight in realistic monolayer FeSe is not determined sorely by the conventional term, and
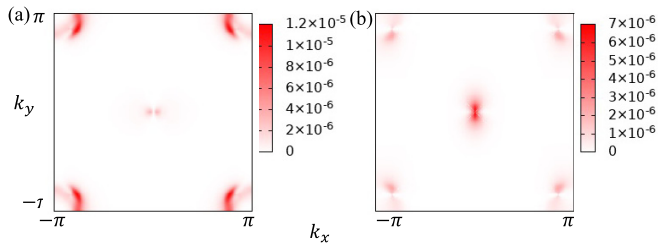
FIG. 3. $\boldsymbol{k}$-resolved contribution to the superfluid weight from (a) the conventional term and (b) the geometric term. The parameters are $n = 6.08$, $z = 1/5$, and $T \approx 2.3$ K.

the geometric properties of Bloch wave functions play an essential role.

To obtain further insights, we show the $\boldsymbol{k}$-resolved contributions of the conventional and geometric terms in Fig. 3. We see significant contributions from near the M point in both terms, as expected from the presence of the Fermi surfaces. Interestingly, there are also sizable contributions from near the Γ point, where the Fermi surface is absent, and it is dominant in the geometric term. This implies that the hole bands below the Fermi level have geometrically nontrivial properties and are essential for enhancing superconductivity in monolayer FeSe.

Next, we discuss superconducting states of $\boldsymbol{k}$-dependent paring. Here, we consider the pairing on the nearest- and next-nearest-neighbor bonds in addition to the on-site pairing. The attractive interaction is assumed as $V_{ij\boldsymbol{k}\boldsymbol{k}'} = V_0 \delta_{ij} + V_1 (\delta_{i,j+5} + \delta_{i+5,j}) \cos k_x/2 \cos k_y/2 \cos k'_x/2 \cos k'_y/2 + V_2 \delta_{ij} (\cos k_x + \cos k_y)(\cos k'_x + \cos k'_y)$, where V_1 and V_2 represent the inter- and intrasublattice attractive interactions, respectively. The superconducting state belongs to the totally symmetric A_{1g} representation irrespective of the parameters V_0, V_1, and V_2. Figure 4 shows the superfluid weight for (a) $V_1 = V_2 = 0.2V_0$ and (b) $V_1 = V_2 = 10V_0$. The gap function is nearly $\boldsymbol{k}$ independent in Fig. 4(a), while it is a highly $\boldsymbol{k}$-dependent in Fig. 4(b). Thus, Figs. 4(a) and 4(b) correspond to the s_{++}-wave and incipient $s_\pm$-wave pairing states, respectively (see Appendix E for details).

In all figures, we can see significant geometric contributions to the superfluid weight as we see in the case of the $\boldsymbol{k}$-independent pairing. Therefore, we conclude that the geometric term plays an essential role in the superconductivity
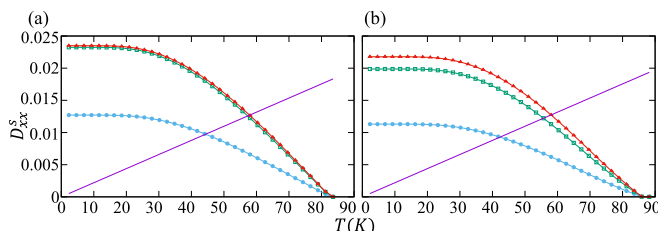

FIG. 4. Superfluid weight for the $\boldsymbol{k}$-dependent gap functions. We set $z = 1/8$ and $n = 6.06$. The attractive interactions are (a) $V_1 = V_2 = 0.2V_0$ and (b) $V_1 = V_2 = 10V_0$. The lines with different colors indicate the same quantities as Fig. 2.

of monolayer FeSe regardless of pairing symmetry. This is also true for the d-wave pairing as shown in Appendix C. On the other hand, the gap term shows a contrasting behavior between the s_{++}-wave pairing and the incipient $s_\pm$-wave pairing. The gap term gives a non-negligible correction in the incipient $s_\pm$-wave state, although it is negligible in the s_{++} state. The contribution to the superfluid weight by the gap term is about 8% and cannot be ignored in the low-temperature regime of Fig. 4(b). Thus, the $\boldsymbol{k}$-dependence in the gap function enhances the superfluid weight and BKT transition temperature through the gap term D^{gap}, which is different from the known effects of thermal excitation due to the anisotropic superconducting gap.

V. CONCLUSION

We formulated the superfluid weight of unconventional superconductors by taking into account the geometric term due to the nontrivial structure of Bloch wave functions and the gap term arising from the $\boldsymbol{k}$-dependence of the gap function. Then, applying the formula to the first-principles model, we found that the geometric properties of Bloch electrons significantly enhance the superconductivity in monolayer FeSe. In particular, the geometric term enhances the BKT transition temperature by nearly 14 K for a typical parameter set.

This high BKT transition temperature can be observed, for example, through the universal jump of the superfluid weight. In our calculations, collecting the data in all figures, we predict the ratio of the universal jump to the total superfluid weight as from 47% to 58%, which the experiments can test. While the enhancement of the BKT transition by interband scatterings was pointed out [87], the geometric properties are completely neglected in Ref. [87]. Thus, the quantum geometric origin clarified here has not been uncovered in such a previous study.

A surprisingly high transition temperature in monolayer FeSe is realized by two origins. One is the enhancement of mean-field transition temperature, probably owing to the excess electron doping or increased electron-phonon coupling [5–7,82–84]. The other is the enhancement of BKT transition temperature attributed not only to the conventional Fermi liquid properties but also to the geometrically nontrivial properties arising from the multiband structure.

The quantum geometrical enhancement of two-dimensional superconductivity is attributed to two necessary conditions: one is suppressing the conventional Fermi liquid term of superfluid weight and the other is the enhancement due to the geometric contribution. The intriguing nature of superconductivity close to the BCS-BEC crossover plays a central role in these properties of monolayer FeSe [88]. Unlike the previous studies on artificial flat-band systems, the former condition is satisfied due to the small Fermi surfaces. The latter is realized by a large Δ/μ and the nontrivial band structure near the Γ point below the Fermi level. Such geometrical enhancement is a universal property of monolayer FeSe, independent of the superconducting symmetry. In conclusion, the monolayer FeSe is an intriguing platform in which the geometric properties of Bloch electrons enhance the superconductivity.

APPENDIX A: DERIVATION OF THE SUPERFLUID WEIGHT

We derive the superfluid weight for unconventional superconductors, including $\boldsymbol{k}$-dependent Cooper pairs, using the Kubo formula and the BCS mean-field theory. For simplicity, we consider the time-reversal symmetric superconductors. First, we derive a formula of the superfluid weight. Then we divide it into four terms. Finally, we show that the conventional term added to the gap term is reduced to the known formula n^*/m^* when $\boldsymbol{\Delta}_{\boldsymbol{k}}^{\dagger} = \boldsymbol{\Delta}_{\boldsymbol{k}} = \mathbf{1} \times \Delta_{\boldsymbol{k}}$, while the geometric term is attributed to the band-resolved quantum metric.

1. Superfluid weight via Kubo formula

We start from a model with an attractive interaction,

$$\hat{H} = \sum_{\boldsymbol{k}} \sum_{ij\sigma} \hat{c}_{i\sigma\boldsymbol{k}}^{\dagger} h_{ij\boldsymbol{k}} \hat{c}_{j\sigma\boldsymbol{k}} + \sum_{\boldsymbol{k}\boldsymbol{k}'} \sum_{ij} \hat{c}_{i\uparrow\boldsymbol{k}}^{\dagger} \hat{c}_{j\downarrow-\boldsymbol{k}}^{\dagger} V_{ij\boldsymbol{k}\boldsymbol{k}'} \hat{c}_{j\downarrow-\boldsymbol{k}'} \hat{c}_{i\uparrow\boldsymbol{k}'}, \tag{A1}$$

where $h_{ij\boldsymbol{k}}$ is the Fourier transform of the hopping integral and $V_{ij\boldsymbol{k}\boldsymbol{k}'}$ represents an attractive interaction. $\hat{c}_{i\sigma\boldsymbol{k}}^{\dagger}$ ($\hat{c}_{i\sigma\boldsymbol{k}}$) is the creation (annihilation) operator, and i, σ, and $\boldsymbol{k}$ represent the orbital and sublattice index, the spin index, and the wave vector, respectively. We apply the BCS mean-field theory to the Hamiltonian:

$$\hat{H} = \sum_{\boldsymbol{k}} \sum_{ij\sigma} \hat{c}_{i\sigma\boldsymbol{k}}^{\dagger} h_{ij\boldsymbol{k}} \hat{c}_{j\sigma\boldsymbol{k}} + \sum_{\boldsymbol{k}} \sum_{ij} (\Delta_{ij\boldsymbol{k}} \hat{c}_{i\uparrow\boldsymbol{k}}^{\dagger} \hat{c}_{j\downarrow-\boldsymbol{k}}^{\dagger} + \text{c.c.})$$
$$- \sum_{\boldsymbol{k}\boldsymbol{k}'} V_{ij\boldsymbol{k}\boldsymbol{k}'} \langle \hat{c}_{i\uparrow\boldsymbol{k}}^{\dagger} \hat{c}_{j\downarrow-\boldsymbol{k}}^{\dagger} \rangle \langle \hat{c}_{j\downarrow-\boldsymbol{k}'} \hat{c}_{i\uparrow\boldsymbol{k}'} \rangle. \tag{A2}$$

Here, the gap function is determined by solving the gap equation:

$$\Delta_{ij\boldsymbol{k}} = \sum_{\boldsymbol{k}'} V_{ij\boldsymbol{k}\boldsymbol{k}'} \langle \hat{c}_{j\downarrow-\boldsymbol{k}'} \hat{c}_{i\uparrow\boldsymbol{k}'} \rangle. \tag{A3}$$

For the superconductivity, we introduce the Nambu spinor,

$$\hat{\boldsymbol{\psi}}_{\boldsymbol{k}}^{\dagger} = (\hat{\boldsymbol{c}}_{\uparrow\boldsymbol{k}}^{\dagger}, \hat{\boldsymbol{c}}_{\downarrow-\boldsymbol{k}}), \tag{A4}$$

$$\hat{\boldsymbol{c}}_{\sigma\boldsymbol{k}}^{\dagger} = (\hat{c}_{1\sigma\boldsymbol{k}}^{\dagger}, \cdots, \hat{c}_{f\sigma\boldsymbol{k}}^{\dagger}), \tag{A5}$$

and the BdG Hamiltonian,

$$H_{\text{BdG}\boldsymbol{k}} = \begin{pmatrix} H_{0\boldsymbol{k}} & \boldsymbol{\Delta}_{\boldsymbol{k}} \\ \boldsymbol{\Delta}_{\boldsymbol{k}}^{\dagger} & -H_{0-\boldsymbol{k}}^{T} \end{pmatrix}, \tag{A6}$$

$$H_{0\boldsymbol{k}} = \begin{pmatrix} h_{11\boldsymbol{k}} & h_{12\boldsymbol{k}} & \cdots & h_{1f\boldsymbol{k}} \\ h_{21\boldsymbol{k}} & h_{22\boldsymbol{k}} & \cdots & h_{2f\boldsymbol{k}} \\ \vdots & \vdots & \ddots & \vdots \\ h_{f1\boldsymbol{k}} & h_{f2\boldsymbol{k}} & \cdots & h_{ff\boldsymbol{k}} \end{pmatrix}. \tag{A7}$$

Here, the dimension f is the total number of the orbital and sublattice degrees of freedom. In the time-reversal symmetric case, $H_{0\boldsymbol{k}} = H_{0-\boldsymbol{k}}^{T}$ is satisfied. We can rewrite the mean-field Hamiltonian as

$$\hat{H} = \sum_{\boldsymbol{k}} \hat{\boldsymbol{\psi}}_{\boldsymbol{k}}^{\dagger} H_{\text{BdG}\boldsymbol{k}} \hat{\boldsymbol{\psi}}_{\boldsymbol{k}} \tag{A8}$$

by ignoring the constant term. We define the Nambu Green function as

$$\boldsymbol{G}(\boldsymbol{k}, \tau - \tau') = \langle T_{\tau}[\hat{\boldsymbol{\psi}}_{\boldsymbol{k}}^{\dagger}(\tau) \otimes \hat{\boldsymbol{\psi}}_{\boldsymbol{k}}(\tau')] \rangle. \tag{A9}$$

Here, $\otimes$ represents the tensor product; the matrix elements for the normal part $i, j \leqslant f$ are defined by $\boldsymbol{G}_{ij}(\boldsymbol{k}, \tau - \tau') = \langle T_{\tau}[\hat{c}_{j\boldsymbol{k}\uparrow}^{\dagger}(\tau) \hat{c}_{i\boldsymbol{k}\uparrow}(\tau')] \rangle$. T_{τ} represents the time ordering product for the imaginary time τ.

The superfluid weight, $D_{\mu\nu}^{\text{s}}$, is defined as the $\boldsymbol{q}$ limit of the Meissner Kernel, $K_{\mu\nu}(\boldsymbol{q}, \omega)$:

$$D_{\mu\nu}^{\text{s}} = \lim_{\boldsymbol{q}\to 0} K_{\mu\nu}(\boldsymbol{q}, 0). \tag{A10}$$

First, we derive the Meissner kernel, which represents the current response to the vector potential:

$$j_{\mu}(\boldsymbol{q}, \omega) = -K_{\mu\nu}(\boldsymbol{q}, \omega) A_{\nu}(\boldsymbol{q}, \omega). \tag{A11}$$

Here, j_{μ} and A_{ν} are the current density and the vector potential, respectively. In the linear response theory, the Meisner Kernel is obtained as,

$$K_{\mu\nu}(\boldsymbol{q}, \tau - \tau') = -K_{\mu\nu}^{\text{para}}(\boldsymbol{q}, \tau - \tau') + K_{\mu\nu}^{\text{dia}}(\boldsymbol{q}, \tau - \tau'), \tag{A12}$$

$$K_{\mu\nu}^{\text{para}}(\boldsymbol{q}, \tau - \tau') = \sum_{\boldsymbol{k}\boldsymbol{k}'} \sum_{\sigma\sigma'} \langle T_{\tau}[\hat{\boldsymbol{c}}_{\sigma\boldsymbol{k}}^{\dagger}(\tau) \partial_{\mu} H_{0\boldsymbol{k}+\boldsymbol{q}/2} \hat{\boldsymbol{c}}_{\sigma\boldsymbol{k}+\boldsymbol{q}}(\tau) \hat{\boldsymbol{c}}_{\sigma'\boldsymbol{k}'}^{\dagger}(\tau') \partial_{\mu} H_{0\boldsymbol{k}'-\boldsymbol{q}/2} \hat{\boldsymbol{c}}_{\sigma\boldsymbol{k}'-\boldsymbol{q}}(\tau')] \rangle, \tag{A13}$$

$$K_{\mu\nu}^{\text{dia}}(\boldsymbol{q}, \tau - \tau') = \sum_{\boldsymbol{k}} \sum_{\sigma} \langle T_{\tau}[\hat{\boldsymbol{c}}_{\sigma\boldsymbol{k}}^{\dagger}(\tau) \partial_{\mu} \partial_{\nu} H_{0\boldsymbol{k}+\boldsymbol{q}/2} \hat{\boldsymbol{c}}_{\sigma\boldsymbol{k}+\boldsymbol{q}}(\tau)] \rangle \delta(\tau - \tau'). \tag{A14}$$

$K_{\mu\nu}^{\text{para}}$ is the paramagnetic term, and $K_{\mu\nu}^{\text{dia}}$ is the diamagnetic term. Using the block diagonal Hamiltonian,

$$H_{p(m)\boldsymbol{k}} = \begin{pmatrix} H_{0\boldsymbol{k}} & 0 \\ 0 & (-)H_{0-\boldsymbol{k}}^{T} \end{pmatrix}, \tag{A15}$$

these terms are written by

$$K_{\mu\nu}^{\mathrm{para}}(\boldsymbol{q}, \tau - \tau') = \sum_{\boldsymbol{k}\boldsymbol{k}'} \left\langle T_\tau \left[\hat{\boldsymbol{\psi}}_{\boldsymbol{k}}^\dagger(\tau) \partial_\mu H_{p\boldsymbol{k}+\boldsymbol{q}/2} \hat{\boldsymbol{\psi}}_{\boldsymbol{k}+\boldsymbol{q}}(\tau) \hat{\boldsymbol{\psi}}_{\boldsymbol{k}'}^\dagger(\tau') \partial_\mu H_{p\boldsymbol{k}'-\boldsymbol{q}/2} \hat{\boldsymbol{\psi}}_{\boldsymbol{k}'-\boldsymbol{q}}(\tau') \right] \right\rangle, \tag{A16}$$

$$K_{\mu\nu}^{\mathrm{dia}}(\boldsymbol{q}, \tau - \tau') = \sum_{\boldsymbol{k}} \left\langle T_\tau \left[\hat{\boldsymbol{\psi}}_{\boldsymbol{k}}^\dagger(\tau) \partial_\mu \partial_\nu H_{m\boldsymbol{k}+\boldsymbol{q}/2} \hat{\boldsymbol{\psi}}_{\boldsymbol{k}+\boldsymbol{q}}(\tau) \right] \right\rangle \delta(\tau - \tau'). \tag{A17}$$

In the Gorkov approximation in which we ignore the vertex correction, these terms are given by the Green's function:

$$K_{\mu\nu}^{\mathrm{para}}(\boldsymbol{q}, \tau - \tau') = - \sum_{\boldsymbol{k}} \mathrm{Tr}[\partial_\mu H_{p\boldsymbol{k}+\boldsymbol{q}/2} \boldsymbol{G}(\boldsymbol{k}, \tau - \tau') \partial_\nu H_{p\boldsymbol{k}+\boldsymbol{q}/2} \boldsymbol{G}(\boldsymbol{k} + \boldsymbol{q}, \tau' - \tau)], \tag{A18}$$

$$K_{\mu\nu}^{\mathrm{dia}}(\boldsymbol{q}, \tau - \tau') = \sum_{\boldsymbol{k}} \mathrm{Tr}[\partial_\mu \partial_\nu H_{m\boldsymbol{k}+\boldsymbol{q}/2} \boldsymbol{G}(\boldsymbol{k}, 0) \delta(\tau - \tau')]. \tag{A19}$$

Trace is taken for the orbital, sublattice, and particle-hole degrees of freedom. After the Fourier transform with respect to the imaginary time, we have

$$K_{\mu\nu}^{\mathrm{para}}(\boldsymbol{q}, \Omega) = - \sum_{\boldsymbol{k}, \omega} \mathrm{Tr}[\partial_\mu H_{p\boldsymbol{k}+\boldsymbol{q}/2} \boldsymbol{G}(\boldsymbol{k}, \omega) \partial_\nu H_{p\boldsymbol{k}+\boldsymbol{q}/2} \boldsymbol{G}(\boldsymbol{k} + \boldsymbol{q}, \omega - \Omega)], \tag{A20}$$

$$K_{\mu\nu}^{\mathrm{dia}}(\boldsymbol{q}, \Omega) = \sum_{\boldsymbol{k}, \omega} \mathrm{Tr}[\partial_\mu \partial_\nu H_{m\boldsymbol{k}+\boldsymbol{q}/2} \boldsymbol{G}(\boldsymbol{k}, \omega)], \tag{A21}$$

where ω and Ω are the Fermionic and Bosonic Matsubara frequencies, respectively. The Nambu Green's function with frequency ω is written as

$$\mathcal{G}(\boldsymbol{k}, \omega) = \frac{1}{i\omega - H_{\mathrm{BdG}\boldsymbol{k}}}. \tag{A22}$$

Using the eigenvalue equation for the BdG Hamiltonian, $H_{\mathrm{BdG}\boldsymbol{k}} |\psi_{\alpha\boldsymbol{k}}\rangle = E_{\alpha\boldsymbol{k}} |\psi_{\alpha\boldsymbol{k}}\rangle$, and taking the limit $\Omega = 0, \boldsymbol{q} \to 0$, we get the formula of the superfluid weight:

$$D_{\mu\nu}^{\mathrm{s}} = -D_{\mu\nu}^{\mathrm{para}} + D_{\mu\nu}^{\mathrm{dia}}, \tag{A23}$$

$$D_{\mu\nu}^{\mathrm{para}} = - \sum_{\boldsymbol{k}} \sum_{\alpha\beta} \frac{f(E_{\alpha\boldsymbol{k}}) - f(E_{\beta\boldsymbol{k}})}{E_{\alpha\boldsymbol{k}} - E_{\beta\boldsymbol{k}}} \langle \psi_{\alpha\boldsymbol{k}} | \partial_\mu H_{p\boldsymbol{k}} | \psi_{\beta\boldsymbol{k}} \rangle \langle \psi_{\beta\boldsymbol{k}} | \partial_\mu H_{p\boldsymbol{k}} | \psi_{\alpha\boldsymbol{k}} \rangle, \tag{A24}$$

$$D_{\mu\nu}^{\mathrm{dia}} = \sum_{\boldsymbol{k}} \sum_{\alpha} f(E_{\alpha\boldsymbol{k}}) \langle \psi_{\alpha\boldsymbol{k}} | \partial_\mu \partial_\nu H_{m\boldsymbol{k}} | \psi_{\alpha\boldsymbol{k}} \rangle. \tag{A25}$$

Equation (A25) for the diamagnetic term can be rewritten as

$$
\begin{aligned}
D_{\mu\nu}^{\mathrm{dia}} = & - \sum_{\boldsymbol{k}} \sum_{\alpha} (\partial_\mu f(E_{\alpha\boldsymbol{k}}) \langle \psi_{\alpha\boldsymbol{k}} | \partial_\nu H_{m\boldsymbol{k}} | \psi_{\alpha\boldsymbol{k}} \rangle \\
& + f(E_{\alpha\boldsymbol{k}}) \langle \partial_\mu \psi_{\alpha\boldsymbol{k}} | \partial_\nu H_{m\boldsymbol{k}} | \psi_{\alpha\boldsymbol{k}} \rangle + f(E_{\alpha\boldsymbol{k}}) \langle \psi_{\alpha\boldsymbol{k}} | \partial_\nu H_{m\boldsymbol{k}} | \partial_\mu \psi_{\alpha\boldsymbol{k}} \rangle), \\
= & - \sum_{\boldsymbol{k}} \sum_{\alpha} (\partial_\mu f(E_{\alpha\boldsymbol{k}}) \langle \psi_{\alpha\boldsymbol{k}} | \partial_\nu H_{m\boldsymbol{k}} | \psi_{\alpha\boldsymbol{k}} \rangle \\
& + f(E_{\alpha\boldsymbol{k}}) \sum_{\beta(\neq\alpha)} \langle \partial_\mu \psi_{\alpha\boldsymbol{k}} | \psi_{\beta\boldsymbol{k}} \rangle \langle \psi_{\beta\boldsymbol{k}} | \partial_\nu H_{m\boldsymbol{k}} | \psi_{\alpha\boldsymbol{k}} \rangle + f(E_{\alpha\boldsymbol{k}}) \sum_{\beta(\neq\alpha)} \langle \psi_{\alpha\boldsymbol{k}} | \partial_\nu H_{m\boldsymbol{k}} | \psi_{\beta\boldsymbol{k}} \rangle \langle \psi_{\beta\boldsymbol{k}} | \partial_\mu \psi_{\alpha\boldsymbol{k}} \rangle), \\
= & - \sum_{\boldsymbol{k}} \sum_{\alpha\beta} \frac{f(E_{\alpha\boldsymbol{k}}) - f(E_{\beta\boldsymbol{k}})}{E_{\alpha\boldsymbol{k}} - E_{\beta\boldsymbol{k}}} \langle \psi_{\alpha\boldsymbol{k}} | \partial_\nu H_{m\boldsymbol{k}} | \psi_{\beta\boldsymbol{k}} \rangle \langle \psi_{\beta\boldsymbol{k}} | \partial_\mu H_{\mathrm{BdG}\boldsymbol{k}} | \psi_{\alpha\boldsymbol{k}} \rangle, \\
= & - \sum_{\boldsymbol{k}} \sum_{\alpha\beta} \frac{f(E_{\alpha\boldsymbol{k}}) - f(E_{\beta\boldsymbol{k}})}{E_{\alpha\boldsymbol{k}} - E_{\beta\boldsymbol{k}}} \langle \psi_{\alpha\boldsymbol{k}} | \partial_\nu H_{m\boldsymbol{k}} | \psi_{\beta\boldsymbol{k}} \rangle \langle \psi_{\beta\boldsymbol{k}} | \partial_\mu H_{m\boldsymbol{k}} | \psi_{\alpha\boldsymbol{k}} \rangle \\
& - \sum_{\boldsymbol{k}} \sum_{\alpha\beta} \frac{f(E_{\alpha\boldsymbol{k}}) - f(E_{\beta\boldsymbol{k}})}{E_{\alpha\boldsymbol{k}} - E_{\beta\boldsymbol{k}}} \langle \psi_{\alpha\boldsymbol{k}} | \partial_\nu H_{m\boldsymbol{k}} | \psi_{\beta\boldsymbol{k}} \rangle \langle \psi_{\beta\boldsymbol{k}} | \partial_\mu \begin{pmatrix} 0 & \boldsymbol{\Delta}_{\boldsymbol{k}} \\ \boldsymbol{\Delta}_{\boldsymbol{k}}^\dagger & 0 \end{pmatrix} | \psi_{\alpha\boldsymbol{k}} \rangle. \tag{A26}
\end{aligned}
$$

Here, we use the relationship, $\langle \partial_\mu \psi_{\alpha k} | \psi_{\alpha k} \rangle + \langle \psi_{\alpha k} | \partial_\mu \psi_{\alpha k} \rangle = 0$ since $\langle \psi_{\alpha k} | \psi_{\alpha k} \rangle = 1$.

2. Superfluid weight based on geometric properties of Bloch electrons

Next, we divide the superfluid weight into four terms based on geometric properties of Bloch electrons. First, we rewrite $|\psi_{\alpha k}\rangle$ using the normal state Bloch wave function. For this purpose, we use the eigenvalue equation of the normal Hamiltonian $H_{0k} |u_{nk}\rangle = \epsilon_{nk} |u_{nk}\rangle$. The unitary matrix which can diagonalize the normal Hamiltonian is written as

$$U_k = (|u_{1k}\rangle, \quad |u_{2k}\rangle, \quad \cdots, \quad |u_{fk}\rangle). \quad (A27)$$

Using this unitary matrix, we get the BdG Hamiltonian of the band representation:

$$\begin{pmatrix} U_k^\dagger & 0 \\ 0 & U_k^\dagger \end{pmatrix} H_{\mathrm{BdG}k} \begin{pmatrix} U_k & 0 \\ 0 & U_k \end{pmatrix} = \begin{pmatrix} U_k^\dagger H_{0k} U_k & U_k^\dagger \mathbf{\Delta}_k U_k \\ U_k^\dagger \mathbf{\Delta}_k^\dagger U_k & -U_k^\dagger H_{0k} U_k \end{pmatrix}. \quad (A28)$$

We consider the unitary matrix which diagonalizes Eq. (A28),

$$\Phi_k = \begin{pmatrix} \phi_{1k}^{1\uparrow} & \phi_{1k}^{2\uparrow} & \cdots & \phi_{1k}^{M\uparrow} \\ \phi_{2k}^{1\uparrow} & \phi_{2k}^{2\uparrow} & \cdots & \phi_{2k}^{M\uparrow} \\ \vdots & \vdots & \ddots & \vdots \\ \phi_{fk}^{1\uparrow} & \phi_{fk}^{2\uparrow} & \cdots & \phi_{fk}^{M\uparrow} \\ \phi_{1k}^{1\downarrow} & \phi_{1k}^{2\downarrow} & \cdots & \phi_{1k}^{M\downarrow} \\ \phi_{2k}^{1\downarrow} & \phi_{2k}^{2\downarrow} & \cdots & \phi_{2k}^{M\downarrow} \\ \vdots & \vdots & \ddots & \vdots \\ \phi_{fk}^{1\downarrow} & \phi_{fk}^{2\downarrow} & \cdots & \phi_{fk}^{M\downarrow} \end{pmatrix}, \quad (A29)$$

with $M = 2 \times f$. Accordingly, we represent $|\psi_{\alpha k}\rangle$ with $|u_{nk}\rangle$:

$$|\psi_{\alpha k}\rangle = \begin{pmatrix} \sum_n \phi_{nk}^{\alpha\uparrow} |u_{nk}\rangle \\ \sum_n \phi_{nk}^{\alpha\downarrow} |u_{nk}\rangle \end{pmatrix}. \quad (A30)$$

Inserting Eq. (A30) to Eq. (A24) and the first term of Eq. (A26), we get

$$2 \sum_k \sum_{\alpha\beta} \sum_{nmls} \frac{f(E_{\alpha k}) - f(E_{\beta k})}{E_{\alpha k} - E_{\beta k}} \phi_{nk}^{*\alpha\uparrow} \phi_{mk}^{\beta\uparrow} \phi_{lk}^{*\beta\downarrow} \phi_{sk}^{\alpha\downarrow} (\langle u_{nk}| \partial_\mu H_{0k} |u_{mk}\rangle \langle u_{lk}| \partial_\nu H_{0k} |u_{sk}\rangle + (\mu \leftrightarrow \nu)). \quad (A31)$$

From the perspective of the interband and intraband contributions, this is divided into three terms:

$$D_{\mu\nu}^{\mathrm{conv}} = 2 \sum_{nmk} C_{nnmmk}^{\uparrow\uparrow\downarrow\downarrow} (\partial_\mu \epsilon_{nk} \partial_\nu \epsilon_{mk} + (\mu \leftrightarrow \nu)), \quad (A32)$$

$$D_{\mu\nu}^{\mathrm{geom}} = 2 \sum_{n\neq m, l\neq s, k} C_{nmlsk}^{\uparrow\uparrow\downarrow\downarrow} (\epsilon_{nk} - \epsilon_{mk})(\epsilon_{lk} - \epsilon_{sk})(\langle \partial_\mu u_{nk}|u_{mk}\rangle \langle u_{lk}|\partial_\nu u_{sk}\rangle + (\mu \leftrightarrow \nu)), \quad (A33)$$

$$D_{\mu\nu}^{\mathrm{multi}} = 2 \sum_{n, l\neq s, k} \left(C_{nnlsk}^{\uparrow\uparrow\downarrow\downarrow} \partial_\mu \epsilon_{nk} (\epsilon_{lk} - \epsilon_{sk}) \langle \partial_\nu u_{lk}|u_{sk}\rangle + C_{lsnnk}^{\uparrow\uparrow\downarrow\downarrow} \partial_\nu \epsilon_{nk} (\epsilon_{lk} - \epsilon_{sk}) \langle \partial_\mu u_{lk}|u_{sk}\rangle + (\mu \leftrightarrow \nu) \right). \quad (A34)$$

Here, we define

$$C_{nmlsk}^{\sigma_1\sigma_2\sigma_3\sigma_4} = \sum_{\alpha\beta} \frac{f(E_{\alpha k}) - f(E_{\beta k})}{E_{\alpha k} - E_{\beta k}} \phi_{nk}^{\alpha\sigma_1*} \phi_{mk}^{\beta\sigma_2} \phi_{lk}^{\beta\sigma_3*} \phi_{sk}^{\alpha\sigma_4}. \quad (A35)$$

Equation (A32) shows the conventional term $D_{\mu\nu}^{\mathrm{conv}}$, which arises from the intraband effect. On the other hand, Eq. (A33) denotes the geometric term $D_{\mu\nu}^{\mathrm{geom}}$, which is purely the interband effect. It should be noticed that $D_{\mu\nu}^{\mathrm{conv}}$ is determined by the band dispersion, while $D_{\mu\nu}^{\mathrm{geom}}$ reflects the geometric properties of the Bloch wave functions. In addition to these terms, we obtain the multigap term, $D_{\mu\nu}^{\mathrm{multi}}$ in Eq. (A34), which comes from the interband pairing effect. In the absence of the interband pairing, this term vanishes. In previous studies, this term has been included in the geometric term [48]. However, from the perspective of the interband and intraband effects, we distinguish this term from the geometric term. Equation (A34) for the multigap term reveals that both intraband and interband effects are needed.

Finally, inserting Eq. (A30) to the second term of Eq. (A26), we get the gap term,

$$D_{\mu\nu}^{\mathrm{gap}} = \sum_{nmlso k} S(C_{nmlsk}^{\uparrow\downarrow\sigma\sigma} \langle u_{nk}| \partial_\mu \mathbf{\Delta}_k |u_{mk}\rangle + C_{nmlsk}^{\downarrow\uparrow\sigma\sigma} \langle u_{nk}| \partial_\mu \mathbf{\Delta}_k^\dagger |u_{mk}\rangle) \langle u_{lk}| \partial_\nu H_{0k} |u_{sk}\rangle, \quad (A36)$$

which comes from the k dependence of the gap function. S takes $-(+)$ when $\sigma = \uparrow (\downarrow)$. Thus, we can divide the superfluid weight into the four tems as $D_{\mu\nu}^s = D_{\mu\nu}^{\mathrm{conv}} + D_{\mu\nu}^{\mathrm{geom}} + D_{\mu\nu}^{\mathrm{multi}} + D_{\mu\nu}^{\mathrm{gap}}$.

3. Superfluid weight in the case of $\mathbf{\Delta}_k = diag(\Delta_k)$

We can simplify the formula for $D_{\mu\nu}^{\mathrm{conv}} + D_{\mu\nu}^{\mathrm{gap}}$ and $D_{\mu\nu}^{\mathrm{geom}}$ when $\mathbf{\Delta}_k = \mathbf{1} \times \Delta_k$. We take a real-valued Δ_k without loss of generality. In this case, the unitary matrix which diagonalizes the BdG Hamiltonian of the band representation can be written in a simple form

$$\phi_{nk}^{i\uparrow} = u_{nk}\delta_{n,i} - v_{nk}\delta_{n+f,i}, \quad (A37)$$

$$\phi_{nk}^{i\downarrow} = v_{nk}\delta_{n,i} + u_{nk}\delta_{n+f,i}, \quad (A38)$$

with

$$u_{nk} = \frac{1}{\sqrt{2}}\sqrt{1 + \frac{\epsilon_{nk}}{E_{nk}}}, \qquad v_{nk} = \frac{1}{\sqrt{2}}\sqrt{1 - \frac{\epsilon_{nk}}{E_{nk}}}, \qquad \text{(A39)}$$

and $E_{nk} = \sqrt{\epsilon_{nk}^2 + \Delta_k^2}$. In this case, the multigap term vanishes since $C_{nmlsk}^{\sigma_1\sigma_2\sigma_3\sigma_4}$ is finite only for $n = s$, $m = l$. Using the above simplification, $D_{\mu\nu}^{\text{conv}}$, $D_{\mu\nu}^{\text{geom}}$, and $D_{\mu\nu}^{\text{gap}}$ are written as

$$D_{\mu\nu}^{\text{conv}} = -\sum_{n\sigma k} \langle u_{nk}| \partial_\mu H_{0k} |u_{nk}\rangle \langle u_{nk}| \partial_\nu H_{0k} |u_{nk}\rangle \left(\sigma \frac{|\Delta_k|^2}{E_{nk}^3} f(\sigma E_{nk}) - \frac{|\Delta_k|^2}{E_{nk}^2} f'(\sigma E_{nk}) \right), \qquad \text{(A40)}$$

$$D_{\mu\nu}^{\text{geom}} = \sum_{n\neq m\sigma\sigma' k} \langle u_{nk}| \partial_\mu H_{0k} |u_{mk}\rangle \langle u_{mk}| \partial_\nu H_{0k} |u_{nk}\rangle \frac{f(\sigma E_{nk}) - f(\sigma' E_{mk})}{\sigma E_{nk} - \sigma' E_{mk}} \left(\sigma\sigma' \frac{|\Delta_k|^2}{E_{nk}E_{mk}} \right), \qquad \text{(A41)}$$

$$D_{\mu\nu}^{\text{gap}} = -\sum_{n\sigma k} \langle u_{nk}| \partial_\mu \boldsymbol{\Delta}_k |u_{nk}\rangle \langle u_{nk}| \partial_\nu H_{0k} |u_{nk}\rangle \left(-\sigma \frac{\Delta_k \epsilon_{nk}}{E_{nk}^3} f(\sigma E_{nk}) + \frac{\Delta_k \epsilon_{nk}}{E_{nk}^2} f'(\sigma E_{nk}) \right), \qquad \text{(A42)}$$

where σ takes ± 1.

At zero temperature, $D_{\mu\nu}^{\text{conv}} + D_{\mu\nu}^{\text{gap}}$ becomes

$$
\begin{aligned}
D_{\mu\nu}^{\text{conv}} + D_{\mu\nu}^{\text{gap}} &= \sum_{nk} \left(\partial_\mu \epsilon_{nk} \partial_\nu \epsilon_{nk} \frac{|\Delta_k|^2}{E_{nk}^3} - \partial_\mu \Delta_k \partial_\nu \epsilon_{nk} \frac{\Delta_k \epsilon_{nk}}{E_{nk}^3} \right), \\
&= \sum_{nk} \partial_\nu \epsilon_{nk} \partial_\mu \left(\frac{\epsilon_{nk}}{E_{nk}} \right), \\
&= -\sum_{nk} \partial_\nu \epsilon_{nk} \partial_\mu \left(1 - \frac{\epsilon_{nk}}{E_{nk}} \right), \\
&= \sum_{nk} \partial_\nu \partial_\mu \epsilon_{nk} \left(1 - \frac{\epsilon_{nk}}{E_{nk}} \right). \qquad \text{(A43)}
\end{aligned}
$$

Note that $(1 - \frac{\epsilon_{nk}}{E_{nk}})$ is the expected value of the particle number and $\partial_\nu \partial_\mu \epsilon_{nk}$ is the inverse mass tensor. Thus, $D_{\mu\nu}^{\text{conv}} + D_{\mu\nu}^{\text{geom}}$ reduces to n^*/m^*. In addition, the geometric term $D_{\mu\nu}^{\text{geom}}$ is written as

$$
\begin{aligned}
D_{\mu\nu}^{\text{geom}} &= \frac{1}{2} \sum_{nm\sigma\sigma' k} (\epsilon_{nk} - \epsilon_{mk})^2 (\langle \partial_\mu u_{nk}|u_{mk}\rangle \langle u_{mk}|\partial_\nu u_{nk}\rangle + \text{c.c.}) \\
&\quad \times \frac{f(\sigma E_{nk}) - f(\sigma' E_{mk})}{\sigma E_{nk} - \sigma' E_{mk}} \left(\sigma\sigma' \frac{|\Delta_k|^2}{E_{nk}E_{mk}} \right), \qquad \text{(A44)}
\end{aligned}
$$

where $(\langle \partial_\mu u_{nk}|u_{mk}\rangle \langle u_{mk}|\partial_\nu u_{nk}\rangle + \text{c.c.})$ is the band-resolved quantum metric. In the isolated-band limit, the geometric term is reduced to the quantum metric in an original sense [24]. We note that Eqs. (A43) and (A44) are valid even for $\boldsymbol{\Delta}_k \neq \mathbf{1} \times \Delta_k$ when the gap function is k independent and the interband pairing is absent. In this case, $E_{nk} = \sqrt{\epsilon_{nk}^2 + |\Delta_n|^2}$ and $\Delta_n = \langle u_{nk}| \boldsymbol{\Delta} |u_{nk}\rangle$.

APPENDIX B: TIGHT-BINDING MODEL REPRODUCING FERMI SURFACES OF FESE

ARPES experiments observed two holelike Fermi surfaces at the Γ point and two electronlike Fermi surfaces at the M point in bulk FeSe [80,81]. However, in the first-principles calculations, the Fermi surfaces are larger than those observed in ARPES and an extra Fermi surface is predicted. Thus, there is a slight discrepancy between the calculations and experiments.

To reproduce the Fermi surfaces of the bulk FeSe observed in the experiments, we slightly modify the hopping parameters given by the first-principles calculation [89–91]. For this purpose, the energies of the d_{xy}-orbital band and the $d_{xz/yz}$-orbital band are shifted by $(-0.28, 0, 0.20)$ and $(-0.27, 0, 0.13)$ at the (Γ, X, M) points in the folded Brillouin zone, respectively. To realize the energy shift, the hopping parameters are changed so as to satisfy

$$\delta E_l(\Gamma) = \delta t_{ll}^{\text{on-site}} + 4\delta t_{ll}^{\text{nn}} + 4\delta t_{ll}^{\text{nnn}}, \qquad \text{(B1)}$$

$$\delta E_l(X) = \delta t_{ll}^{\text{on-site}}, \qquad \text{(B2)}$$

$$\delta E_l(M) = \delta t_{ll}^{\text{on-site}} - 4\delta t_{ll}^{\text{nnn}}, \qquad \text{(B3)}$$

where we represent the energy shifts of the l-orbital band at the Γ, X, and M points as $\delta E_l(\Gamma)$, $\delta E_l(X)$ and $\delta E_l(M)$, respectively. The modification in the intraorbital hopping integral is represented by δt_{ll}, and on-site, nn, and nnn denote the on-site, first-nearest-neighbor, and second-nearest-neighbor hoppings, respectively. In the ten-orbital model with two sublattices in the unit cell, $\delta t_{ll}^{\text{nn}}$ ($\delta t_{ll}^{\text{nnn}}$) is the intersublattice (intrasublattice) hopping. We also tune the chemical potential so the extra Fermi surface near the Γ point vanishes and the fillings are $n = 6.06, 6.08, 6.1$. Using these parameters, we can reproduce the Fermi surfaces of monolayer FeSe grown on SrTiO$_3$.

APPENDIX C: SUPERFLUID WEIGHT IN THE *D*-WAVE PAIRING STATE

Since the d-wave pairing state is one of the representative candidates for superconducting symmetry in monolayer FeSe, we here study the superfluid weight in the d-wave pairing state, using the pairing interaction

$$V_{ijkk'} = V_1(\delta_{i,j+5} + \delta_{i+5,j}) \sin k_x/2 \sin k_y/2 \sin k_x'/2 \sin k_y'/2, \qquad \text{(C1)}$$

which stabilizes the gap function belonging to the B_{1g} irreducible representation.

The temperature dependence of the superfluid weight is shown in Fig. 5. A sizable geometric contribution is confirmed, and we conclude that the quantum geometric enhancement of superconductivity is a universal property of monolayer FeSe, independent of pairing symmetry. On the other hand, since the gap function $\Delta(\boldsymbol{k}) \propto \sin k_x/2 \sin k_y/2$
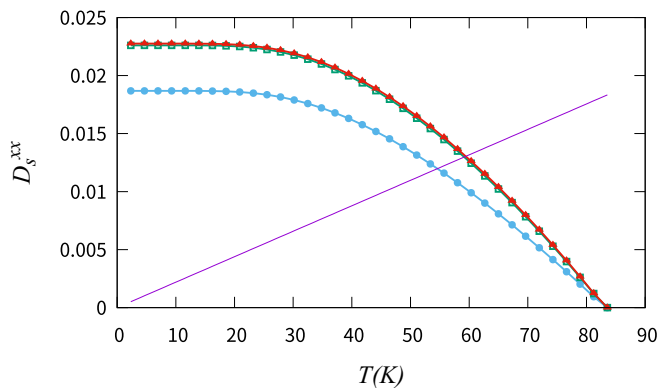
FIG. 5. Superfluid weight in the d-wave pairing state. Here, we set the parameters as $n = 6.08$, $z = 1/5$, and $T_c \approx 83$ K.

vanishes at the Γ point, the geometric contribution from near the Γ point, which is sizable in the case of s-wave symmetry, is suppressed. Therefore, the total geometric contribution in the d-wave pairing state is smaller than that in the s-wave pairing state. This result supports the importance of the band near the Γ point, which is below the Fermi level in monolayer FeSe.

APPENDIX D: SUPERFLUID WEIGHT FOR $T_C = 65K$ WITH THE FIRST-PRINCIPLES MODEL

In this Appendix, we show the superfluid weight for the mean-field superconducting transition temperature $T_c \approx 65$ K using the ten-orbital tight-binding model. In the main text, we show the results for $T_c \approx 83$ K. Below we see qualitatively the same results.

For simplicity, we consider the $\mathbf{k}$-independent pairing, given by an on-site pairing interaction $V_{ijk} = V_0 \delta_{ij}$, in this Appendix. The temperature dependence of the superfluid weight is shown in Fig. 6. In all panels, the geometric term gives a sizable correction to the superfluid weight. In Fig. 6(b), the geometric term determines the superfluid weight about 32% at $T \approx 2.3$ K. The magnitude of the gap function on the Fermi surface is nearly 9.3 meV in Fig. 6(b), while its experimental values are reported as at most 20 meV [1] and at least 8 meV [82]. Thus, a larger gap function may be realized in monolayer FeSe. For a larger T_c and gap function, a more significant geometric contribution to the superfluid weight is obtained, as we see in the main text.

APPENDIX E: GAP FUNCTION IN THE S-WAVE AND INCIPIENT S_{+-}-WAVE STATES

Here, we explain the relationship between the gap function and the pairing interaction adopted in this paper. A highly $\mathbf{k}$-dependent gap function may show the sign change between the Γ and M points. Such a gap function corresponds to the incipient s_{+-}-wave pairing state proposed for monolayer FeSe in previous studies [5]. On the other hand, the weakly $\mathbf{k}$-dependent gap function does not show the sign change, which is regarded as the s_{++}-wave pairing state.

We consider the $\mathbf{k}$-dependent pairing interaction,

$$\begin{aligned} V_{ijkk'} = {} & V_0 \delta_{ij} + V_1 (\delta_{i,j+5} + \delta_{i+5,j}) \cos k_x/2 \\ & \times \cos k_y/2 \cos k'_x/2 \cos k'_y/2 \\ & + V_2 \delta_{ij} (\cos k_x + \cos k_y)(\cos k'_x + \cos k'_y), \quad \text{(E1)} \end{aligned}$$
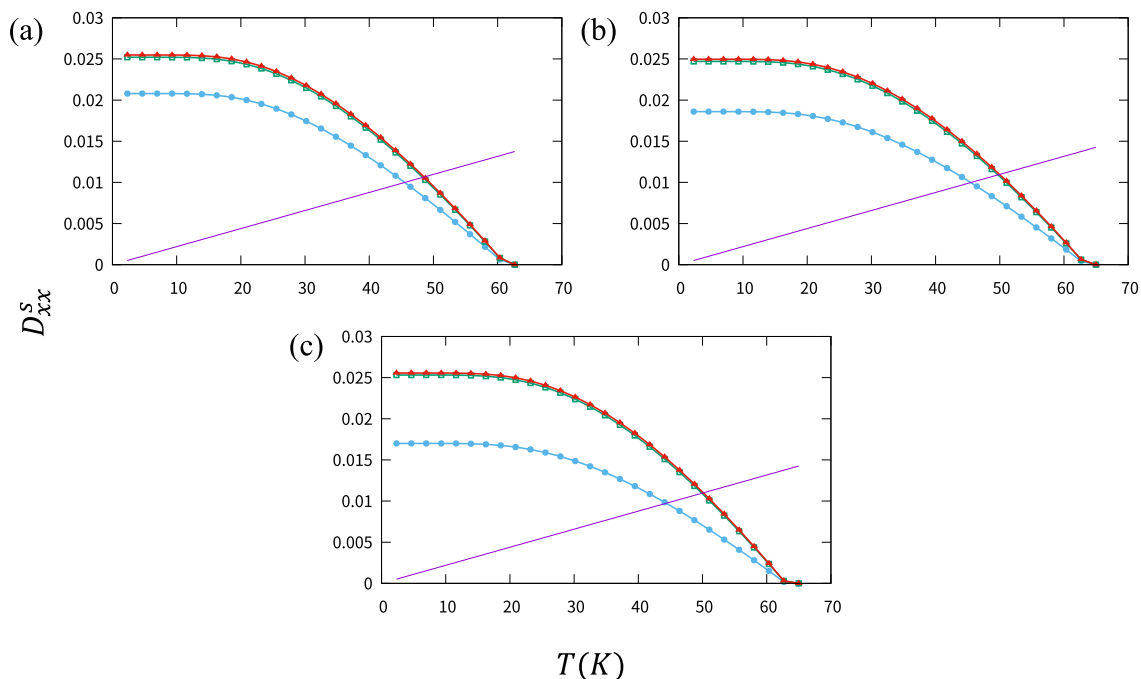

FIG. 6. Temperature dependence of the superfluid weight for $\mathbf{k}$-independent pairing and $z = 1/5$. The blue, green, and red lines show the conventional term (D^{conv}), conventional + geometric term ($D^{\text{geom}} + D^{\text{conv}}$), and the total superfluid weight (D^s), respectively. The purple line shows $8T/\pi$. The intersection between the purple line and the red line shows the BKT transition temperature. (a)–(c) are for $n = 6.1$, 6.08, and 6.06, respectively.
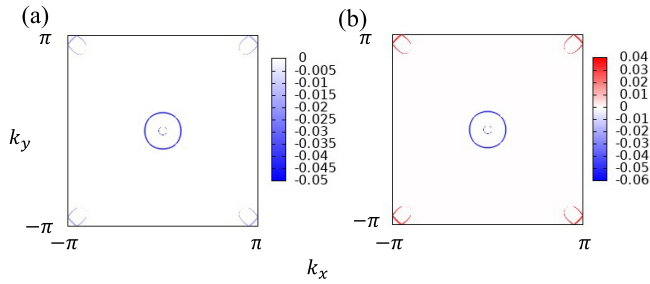
FIG. 7. Gap function on the Fermi surfaces, defined as $\sum_{m,n} 4T^2 \langle u_{nk}| \boldsymbol{\Delta} |u_{mk}\rangle \times f'(\epsilon_{nk}^{\text{bulk}}) f'(\epsilon_{mk}^{\text{bulk}})$. Here, $\epsilon_{nk}^{\text{bulk}}$ is the single-particle energy of the bulk FeSe. The attractive interaction is (a) $V_1 = V_2 = 0.2V_0$ and (b) $V_1 = V_2 = 10V_0$. From the panels, we find that (a) shows the s_{++}-wave pairing state while (b) shows the incipient s_{+-}-wave state.

where the pairing interaction on the nearest- and next-nearest-neighbor bonds is taken into account in addition to the on-site pairing interaction. In Fig. 7, we plot the gap function on the Fermi surfaces for $n = 6$. The parameters for the interaction are (a) $V_1 = V_2 = 0.2V_0$ and (b) $V_1 = V_2 = 10V_0$, as we adopted in the main text. As we see from Fig. 7, the sign of the gap function is the same between the Γ and M points in Fig. 7(a), although it is opposite in Fig. 7(b). Thus, the pairing interaction for Fig. 7(a) leads to the s_{++}-wave pairing state, while that for Fig. 7(b) to the incipient s_{+-}-wave pairing state. Note that the hole Fermi surfaces near the Γ point vanish when $n \geqslant 6.06$ due to the electron doping as we adopt in the main text. In this case, there is no sign change on the remaining Fermi surfaces, although the sign reversal of the gap function manifests on bands slightly below the Fermi level and may affect some properties [62,68–70].

[1] Q.-Y. Wang, Z. Li, W.-H. Zhang, Z.-C. Zhang, J.-S. Zhang, W. Li, H. Ding, Y.-B. Ou, P. Deng, K. Chang, J. Wen, C.-L. Song, K. He, J.-F. Jia, S.-H. Ji, Y.-Y. Wang, L.-L. Wang, X. Chen, X.-C. Ma, and Q.-K. Xue, Interface-induced high-temperature superconductivity in single unit-cell FeSe films on SrTiO$_3$, Chin. Phys. Lett. **29**, 037402 (2012).

[2] S. He, J. He, W. Zhang, L. Zhao, D. Liu, X. Liu, D. Mou, Y.-B. Ou, Q.-Y. Wang, Z. Li, L. Wang, Y. Peng, Y. Liu, C. Chen, L. Yu, G. Liu, X. Dong, J. Zhang, C. Chen, Z. Xu *et al.*, Phase diagram and electronic indication of high-temperature superconductivity at 65 k in single-layer FeSe films, Nat. Mater. **12**, 605 (2013).

[3] Y. Xu, H. Rong, Q. Wang, D. Wu, Y. Hu, Y. Cai, Q. Gao, H. Yan, C. Li, C. Yin, H. Chen, J. Huang, Z. Zhu, Y. Huang, G. Liu, Z. Xu, L. Zhao, and X. J. Zhou, Spectroscopic evidence of superconductivity pairing at 83 k in single-layer FeSe/SrTiO$_3$ films, Nat. Commun. **12**, 2840 (2021).

[4] F.-C. Hsu, J.-Y. Luo, K.-W. Yeh, T.-K. Chen, T.-W. Huang, P. M. Wu, Y.-C. Lee, Y.-L. Huang, Y.-Y. Chu, D.-C. Yan, and M.-K. Wu, Superconductivity in the PBo-type structure α-FeSe, Proc. Natl. Acad. Sci. **105**, 14262 (2008).

[5] D. Huang and J. E. Hoffman, Monolayer FeSe on SrTiO$_3$, Annu. Rev. Condens. Matter Phys. **8**, 311 (2017).

[6] J. J. Lee, F. T. Schmitt, R. G. Moore, S. Johnston, Y.-T. Cui, W. Li, M. Yi, Z. K. Liu, M. Hashimoto, Y. Zhang, D. H. Lu, T. P. Devereaux, D.-H. Lee, and Z.-X. Shen, Interfacial mode coupling as the origin of the enhancement of T$_C$ in FeSe films on SrTiO$_3$, Nature (London) **515**, 245 (2014).

[7] Q. Song, T. L. Yu, X. Lou, B. P. Xie, H. C. Xu, C. H. P. Wen, Q. Yao, S. Y. Zhang, X. T. Zhu, J. D. Guo, R. Peng, and D. L. Feng, Evidence of cooperative effect on the enhanced superconducting transition temperature at the FeSe/SrTiO$_3$ interface, Nat. Commun. **10**, 758 (2019).

[8] C.-L. Song, Y.-L. Wang, Y.-P. Jiang, Z. Li, L. Wang, K. He, X. Chen, X.-C. Ma, and Q.-K. Xue, Molecular-beam epitaxy and robust superconductivity of stoichiometric FeSe crystalline films on bilayer graphene, Phys. Rev. B **84**, 020503 (2011).

[9] For example, different from the SrTiO$_3$ substrate, the graphene substrate suppresses the mean-field transition temperature [8].

[10] J. M. Kosterlitz and D. J. Thouless, Ordering, metastability and phase transitions in two-dimensional systems, J. Phys. C **6**, 1181 (1973).

[11] V. L. Berezinskii, Destruction of long-range order in one- dimensional and two-dimensional systems having a continuous symmetry group i. Classical systems, Sov. Phys. JETP **34**, 493 (1972).

[12] M. R. Beasley, J. E. Mooij, and T. P. Orlando, Possibility of Vortex-Antivortex Pair Dissociation in Two-Dimensional Superconductors, Phys. Rev. Lett. **42**, 1165 (1979).

[13] Y. Cao, S.-H. Zou, X.-J. Liu, S. Yi, G.-L. Long, and H. Hu, Gapless Topological Fulde-Ferrell Superfluidity in Spin-Orbit Coupled Fermi Gases, Phys. Rev. Lett. **113**, 115302 (2014).

[14] G. A. Williams and E. Varoquaux, Vortex pair energy in an anisotropic superfluid film, J. Low Temp. Phys. **113**, 405 (1998).

[15] P. K. Biswas, Z. Salman, Q. Song, R. Peng, J. Zhang, L. Shu, D. L. Feng, T. Prokscha, and E. Morenzoni, Direct evidence of superconductivity and determination of the superfluid density in buried ultrathin FeSe grown on 3SrTiO$_3$, Phys. Rev. B **97**, 174509 (2018).

[16] G. Yao, M.-C. Duan, N. Liu, Y. Wu, D.-D. Guan, S. Wang, H. Zheng, Y.-Y. Li, C. Liu, and J.-F. Jia, Diamagnetic Response of Potassium-Adsorbed Multilayer FeSe Film, Phys. Rev. Lett. **123**, 257001 (2019).

[17] R. Khasanov, M. Bendele, A. Amato, K. Conder, H. Keller, H.-H. Klauss, H. Luetkens, and E. Pomjakushina, Evolution of Two-Gap Behavior of the Superconductor FeSe$_{1-x}$, Phys. Rev. Lett. **104**, 087004 (2010).

[18] H. Takahashi, Y. Imai, S. Komiya, I. Tsukada, and A. Maeda, Anomalous temperature dependence of the superfluid density caused by a dirty-to-clean crossover in superconducting FeSe$_{0.4}$Te$_{0.6}$ single crystals, Phys. Rev. B **84**, 132503 (2011).

[19] P. K. Biswas, A. Kreisel, Q. Wang, D. T. Adroja, A. D. Hillier, J. Zhao, R. Khasanov, J.-C. Orain, A. Amato, and E. Morenzoni, Evidence of nodal gap structure in the basal plane of the FeSe superconductor, Phys. Rev. B **98**, 180501 (2018).

[20] T. Jujo, Fermi liquid theory on transport phenomena in the superconducting state, J. Phys. Soc. Jpn. **70**, 1349 (2001).

[21] M. Tinkham, *Introduction to Superconductivity*, 2nd ed. (Dover Publications, New York, 2004)

[22] Strictly speaking, the quantum correction due to interactions also affects the superfluid weight [20]. We avoid explicitly showing it and include it into the effective mass.

[23] S. Peotta and P. Törmä, Superfluidity in topologically nontrivial flat bands, Nat. Commun. **6**, 8944 (2015).

[24] L. Liang, T. I. Vanhala, S. Peotta, T. Siro, A. Harju, and P. Törmä, Band geometry, Berry curvature, and superfluid weight, Phys. Rev. B **95**, 024515 (2017).

[25] R. Resta, The insulating state of matter: A geometrical theory, Eur. Phys. J. B **79**, 121 (2011).

[26] J. P. Provost and G. Vallee, Riemannian structure on manifolds of quantum states, Commun. Math. Phys. **76**, 289 (1980).

[27] M. V. Berry, Quantal phase factors accompanying adiabatic changes, Proceedings of the Royal Society of London. A. Math. Phys. Sci. **392**, 45 (1984).

[28] D. J. Thouless, M. Kohmoto, M. P. Nightingale, and M. den Nijs, Quantized Hall Conductance in a Two-Dimensional Periodic Potential, Phys. Rev. Lett. **49**, 405 (1982).

[29] D. Xiao, M.-C. Chang, and Q. Niu, Berry phase effects on electronic properties, Rev. Mod. Phys. **82**, 1959 (2010).

[30] N. Nagaosa, J. Sinova, S. Onoda, A. H. MacDonald, and N. P. Ong, Anomalous Hall effect, Rev. Mod. Phys. **82**, 1539 (2010).

[31] N. Marzari and D. Vanderbilt, Maximally localized generalized Wannier functions for composite energy bands, Phys. Rev. B **56**, 12847 (1997).

[32] T. Neupert, C. Chamon, and C. Mudry, Measuring the quantum geometry of Bloch bands with current noise, Phys. Rev. B **87**, 245103 (2013).

[33] A. Srivastava and A. m. c. Imamoğlu, Signatures of Bloch-Band Geometry on Excitons: Nonhydrogenic Spectra in Transition-Metal Dichalcogenides, Phys. Rev. Lett. **115**, 166802 (2015).

[34] Y. Gao, S. A. Yang, and Q. Niu, Field Induced Positional Shift of Bloch Electrons and Its Dynamical Implications, Phys. Rev. Lett. **112**, 166601 (2014).

[35] Y. Gao and D. Xiao, Nonreciprocal Directional Dichroism Induced by the Quantum Metric Dipole, Phys. Rev. Lett. **122**, 227402 (2019).

[36] M. F. Lapa and T. L. Hughes, Semiclassical wave packet dynamics in nonuniform electric fields, Phys. Rev. B **99**, 121111 (2019).

[37] A. Daido, A. Shitade, and Y. Yanase, Thermodynamic approach to electric quadrupole moments, Phys. Rev. B **102**, 235149 (2020).

[38] J. Ahn, G.-Y. Guo, and N. Nagaosa, Low-Frequency Divergence and Quantum Geometry of the Bulk Photovoltaic Effect in Topological Semimetals, Phys. Rev. X **10**, 041041 (2020).

[39] H. Watanabe and Y. Yanase, Chiral Photocurrent in Parity-Violating Magnet and Enhanced Response in Topological Antiferromagnet, Phys. Rev. X **11**, 011001 (2021).

[40] A. Julku, S. Peotta, T. I. Vanhala, D.-H. Kim, and P. Törmä, Geometric Origin of Superfluidity in the Lieb-Lattice Flat Band, Phys. Rev. Lett. **117**, 045303 (2016).

[41] P. He, H.-T. Ding, and S.-L. Zhu, Geometry and superfluidity of the flat band in a non-Hermitian optical lattice, Phys. Rev. A **103**, 043329 (2021).

[42] S. Taie, H. Ozawa, T. Ichinose, T. Nishio, S. Nakajima, and Y. Takahashi, Coherent driving and freezing of bosonic matter wave in an optical Lieb lattice, Sci. Adv. **1**, e1500854 (2015).

[43] H. Ozawa, S. Taie, T. Ichinose, and Y. Takahashi, Interaction-Driven Shift and Distortion of a Flat Band in an Optical Lieb Lattice, Phys. Rev. Lett. **118**, 175301 (2017).

[44] Y. Cao, V. Fatemi, S. Fang, K. Watanabe, T. Taniguchi, E. Kaxiras, and P. Jarillo-Herrero, Unconventional superconductivity in magic-angle graphene superlattices, Nature (London) **556**, 43 (2018).

[45] G. Li, A. Luican, J. M. B. Lopes dos Santos, A. H. Castro Neto, A. Reina, J. Kong, and E. Y. Andrei, Observation of Van Hove singularities in twisted graphene layers, Nat. Phys. **6**, 109 (2010).

[46] R. Bistritzer and A. H. MacDonald, Moiré bands in twisted double-layer graphene, Proc. Natl. Acad. Sci. **108**, 12233 (2011).

[47] X. Hu, T. Hyart, D. I. Pikulin, and E. Rossi, Geometric and Conventional Contribution to the Superfluid Weight in Twisted Bilayer Graphene, Phys. Rev. Lett. **123**, 237002 (2019).

[48] A. Julku, T. J. Peltonen, L. Liang, T. T. Heikkilä, and P. Törmä, Superfluid weight and Berezinskii-Kosterlitz-Thouless transition temperature of twisted bilayer graphene, Phys. Rev. B **101**, 060505 (2020).

[49] F. Xie, Z. Song, B. Lian, and B. A. Bernevig, Topology-Bounded Superfluid Weight in Twisted Bilayer Graphene, Phys. Rev. Lett. **124**, 167002 (2020).

[50] Z. Wang, G. Chaudhary, Q. Chen, and K. Levin, Quantum geometric contributions to the BKT transition: Beyond mean field theory, Phys. Rev. B **102**, 184504 (2020).

[51] Z. Wang, P. Zhang, G. Xu, L. K. Zeng, H. Miao, X. Xu, T. Qian, H. Weng, P. Richard, A. V. Fedorov, H. Ding, X. Dai, and Z. Fang, Topological nature of the FeSe$_{0.5}$Te$_{0.5}$ superconductor, Phys. Rev. B **92**, 115119 (2015).

[52] G. Xu, B. Lian, P. Tang, X.-L. Qi, and S.-C. Zhang, Topological Superconductivity on the Surface of Fe-Based Superconductors, Phys. Rev. Lett. **117**, 047001 (2016).

[53] D. Wang, L. Kong, P. Fan, H. Chen, S. Zhu, W. Liu, L. Cao, Y. Sun, S. Du, J. Schneeloch, R. Zhong, G. Gu, L. Fu, H. Ding, and H.-J. Gao, Evidence for Majorana bound states in an iron-based superconductor, Science **362**, 333 (2018).

[54] P. Zhang, K. Yaji, T. Hashimoto, Y. Ota, T. Kondo, K. Okazaki, Z. Wang, J. Wen, G. D. Gu, H. Ding, and S. Shin, Observation of topological superconductivity on the surface of an iron-based superconductor, Science **360**, 182 (2018).

[55] T. Machida, Y. Sun, S. Pyon, S. Takeda, Y. Kohsaka, T. Hanaguri, T. Sasagawa, and T. Tamegai, Zero-energy vortex bound state in the superconducting topological surface state of fe(se,te), Nat. Mater. **18**, 811 (2019).

[56] P. Noziöres and S. Schmitt-Rink, Bose condensation in an attractive fermion gas: From weak to strong coupling superconductivity, J. Low Temp. Phys. **59**, 195 (1985).

[57] S. Kasahara, T. Watashige, T. Hanaguri, Y. Kohsaka, T. Yamashita, Y. Shimoyama, Y. Mizukami, R. Endo, H. Ikeda, K. Aoyama, T. Terashima, S. Uji, T. Wolf, H. von Löhneysen, T. Shibauchi, and Y. Matsuda, Field-induced superconducting phase of FeSe in the BCS-BEC cross-over, Proc. Natl. Acad. Sci. **111**, 16309 (2014).

[58] S. Kasahara, T. Yamashita, A. Shi, R. Kobayashi, Y. Shimoyama, T. Watashige, K. Ishida, T. Terashima, T. Wolf, F. Hardy, C. Meingast, H. v. Löhneysen, A. Levchenko, T. Shibauchi, and Y. Matsuda, Giant superconducting fluctuations

in the compensated semimetal FeSe at the BCS-BEC crossover, Nat. Commun. **7**, 12843 (2016).

[59] T. Hanaguri, S. Kasahara, J. Böker, I. Eremin, T. Shibauchi, and Y. Matsuda, Quantum Vortex Core and Missing Pseudogap in the Multiband BCS-BEC Crossover Superconductor FeSe, Phys. Rev. Lett. **122**, 077001 (2019).

[60] S. Kasahara, Y. Sato, S. Licciardello, M. Čulo, S. Arsenijević, T. Ottenbros, T. Tominaga, J. Böker, I. Eremin, T. Shibauchi, J. Wosnitza, N. E. Hussey, and Y. Matsuda, Evidence for an Fulde-Ferrell-Larkin-Ovchinnikov State with Segmented Vortices in the BCS-BEC-Crossover Superconductor FeSe, Phys. Rev. Lett. **124**, 107001 (2020).

[61] Y. Yamakawa and H. Kontani, Superconductivity without a hole pocket in electron-doped FeSe: Analysis beyond the Migdal-Eliashberg formalism, Phys. Rev. B **96**, 045130 (2017).

[62] Y. Gao, Y. Yu, T. Zhou, H. Huang, and Q.-H. Wang, Hidden sign-changing s-wave superconductivity in monolayer FeSe, Phys. Rev. B **94**, 144512 (2016).

[63] M. Khodas and A. V. Chubukov, Interpocket Pairing and Gap Symmetry in Fe-Based Superconductors with Only Electron Pockets, Phys. Rev. Lett. **108**, 247003 (2012).

[64] X. Chen, S. Maiti, A. Linscheid, and P. J. Hirschfeld, Electron pairing in the presence of incipient bands in iron-based superconductors, Phys. Rev. B **92**, 224514 (2015).

[65] J. Kang and R. M. Fernandes, Superconductivity in FeSe Thin Films Driven by the Interplay Between Nematic Fluctuations and Spin-Orbit Coupling, Phys. Rev. Lett. **117**, 217003 (2016).

[66] A. Aperis and P. M. Oppeneer, Multiband full-bandwidth anisotropic Eliashberg theory of interfacial electron-phonon coupling and high$-t_c$ superconductivity in FeSe/SrTiO$_3$, Phys. Rev. B **97**, 060501 (2018).

[67] Q. Fan, W. H. Zhang, X. Liu, Y. J. Yan, M. Q. Ren, R. Peng, H. C. Xu, B. P. Xie, J. P. Hu, T. Zhang, and D. L. Feng, Plain s-wave superconductivity in single-layer FeSe on SrTiO$_3$ probed by scanning tunnellingÂ microscopy, Nat. Phys. **11**, 946 (2015).

[68] Y. Bang, Phonon boost effect on the $s^\pm$-wave superconductor with incipient band, Sci. Rep. **9**, 3907 (2019).

[69] T. A. Maier, V. Mishra, G. Balduzzi, and D. J. Scalapino, Effective pairing interaction in a system with an incipient band, Phys. Rev. B **99**, 140504 (2019).

[70] L. Rademaker, G. Alvarez-Suchini, K. Nakatsukasa, Y. Wang, and S. Johnston, Enhanced superconductivity in FeSe/SrTio$_3$ from the combination of forward scattering phonons and spin fluctuations, Phys. Rev. B **103**, 144504 (2021).

[71] Y.-Y. Xiang, F. Wang, D. Wang, Q.-H. Wang, and D.-H. Lee, High-temperature superconductivity at the FeSe/SrTiO$_3$ interface, Phys. Rev. B **86**, 134508 (2012).

[72] Y.-Y. Xiang, Y. Yang, W.-S. Wang, Z.-Z. Li, and Q.-H. Wang, Functional renormalization group study of pairing symmetry and pairing mechanism in iron-selenide superconductors, Phys. Rev. B **88**, 104516 (2013).

[73] D. F. Agterberg, T. Shishidou, J. O'Halloran, P. M. R. Brydon, and M. Weinert, Resilient Nodeless d-Wave Superconductivity in Monolayer FeSe, Phys. Rev. Lett. **119**, 267001 (2017).

[74] Z. Ge, C. Yan, H. Zhang, D. Agterberg, M. Weinert, and L. Li, Evidence for d-wave superconductivity in single layer FeSe/SrTiO$_3$ probed by quasiparticle scattering off step edges, Nano Lett. **19**, 2497 (2019).

[75] F. Schrodi, A. Aperis, and P. M. Oppeneer, Multichannel superconductivity of monolayer FeSe on SrTiO$_3$: Interplay of spin fluctuations and electron-phonon interaction, Phys. Rev. B **102**, 180501 (2020).

[76] Y. Zhang, J. J. Lee, R. G. Moore, W. Li, M. Yi, M. Hashimoto, D. H. Lu, T. P. Devereaux, D.-H. Lee, and Z.-X. Shen, Superconducting Gap Anisotropy in Monolayer FeSe Thin Film, Phys. Rev. Lett. **117**, 117001 (2016).

[77] P. Blaha, K. Schwarz, G. K H Madsen, D. Kvasnicka, J. Luitz, R. Laskowsk, F. Tran, L. Marks, and L. Marks, *WIEN2k: An Augmented Plane Wave Plus Local Orbitals Program for Calculating Crystal Properties* (Techn. Universitat, Wien, Austria, 2019).

[78] I. Souza, N. Marzari, and D. Vanderbilt, Maximally localized Wannier functions for entangled energy bands, Phys. Rev. B **65**, 035109 (2001).

[79] A. A. Mostofi, J. R. Yates, Y.-S. Lee, I. Souza, D. Vanderbilt, and N. Marzari, wannier90: A tool for obtaining maximally-localised Wannier functions, Comput. Phys. Commun. **178**, 685 (2008).

[80] J. Maletz, V. B. Zabolotnyy, D. V. Evtushinsky, S. Thirupathaiah, A. U. B. Wolter, L. Harnagea, A. N. Yaresko, A. N. Vasiliev, D. A. Chareev, A. E. Böhmer, F. Hardy, T. Wolf, C. Meingast, E. D. L. Rienks, B. Büchner, and S. V. Borisenko, Unusual band renormalization in the simplest iron-based superconductor FeSe$_{1-x}$, Phys. Rev. B **89**, 220506 (2014).

[81] Y. Zhang, M. Yi, Z.-K. Liu, W. Li, J. J. Lee, R. G. Moore, M. Hashimoto, M. Nakajima, H. Eisaki, S.-K. Mo, Z. Hussain, T. P. Devereaux, Z.-X. Shen, and D. H. Lu, Distinctive orbital anisotropy observed in the nematic state of a FeSe thin film, Phys. Rev. B **94**, 115153 (2016).

[82] Y. Miyata, K. Nakayama, K. Sugawara, T. Sato, and T. Takahashi, High-temperature superconductivity in potassium-coated multilayer FeSe thin films, Nat. Mater. **14**, 775 (2015).

[83] K. Hanzawa, H. Sato, H. Hiramatsu, T. Kamiya, and H. Hosono, Electric field-induced superconducting transition of insulating FeSe thin film at 35 k, Proc. Natl. Acad. Sci. **113**, 3986 (2016).

[84] J. Shiogai, Y. Ito, T. Mitsuhashi, T. Nojima, and A. Tsukazaki, Electric-field-induced superconductivity in electrochemically etched ultrathin FeSe films on SrTiO$_3$ and mgo, Nat. Phys. **12**, 42 (2016).

[85] M. Aichhorn, S. Biermann, T. Miyake, A. Georges, and M. Imada, Theoretical evidence for strong correlations and incoherent metallic state in FeSe, Phys. Rev. B **82**, 064504 (2010).

[86] Z. P. Yin, K. Haule, and G. Kotliar, Kinetic frustration and the nature of the magnetic and paramagnetic states in iron pnictides and ironÂ chalcogenides, Nat. Mater. **10**, 932 (2011).

[87] A. V. Chubukov, I. Eremin, and D. V. Efremov, Superconductivity versus bound-state formation in a two-band superconductor with small Fermi energy: Applications to Fe pnictides/chalcogenides and doped SrTiO$_3$, Phys. Rev. B **93**, 174516 (2016).

[88] This implies that other iron-based superconductors may not have the superfluid weight with geometric origin because of a significant conventional contribution, although iron-based superconductors ubiquitously show geometric properties [92].

[89] Y. Yamakawa, S. Onari, and H. Kontani, Nematicity and Magnetism in FeSe and Other Families of Fe-Based Superconductors, Phys. Rev. X **6**, 021032 (2016).

[90] S. Onari, Y. Yamakawa, and H. Kontani, Sign-Reversing Orbital Polarization in the Nematic Phase of FeSe Due to the C_2 Symmetry Breaking in the Self-Energy, Phys. Rev. Lett. **116**, 227001 (2016).

[91] J. Ishizuka, T. Yamada, Y. Yanagi, and Y. Åno, Fermi surface, pressure-induced antiferromagnetic order, and superconductivity in FeSe, J. Phys. Soc. Jpn. **87**, 014705 (2018).

[92] T. Kitamura, J. Ishizuka, A. Daido, and Y. Yanase, Thermodynamic electric quadrupole moments of nematic phases from first-principles calculations, Phys. Rev. B **103**, 245114 (2021).